Engineering Structures 148 (2017) 924–935

Contents lists available at ScienceDirect

Engineering Structures

journal homepage: www.elsevier.com/locate/engstruct

Damage detection, localization and quantification in conductive smart concrete structures using a resistor mesh model

Austin Downey [a,*], Antonella D'Alessandro [b], Micah Baquera [c], Enrique García-Macías [d], Daniel Rolfes [e], Filippo Ubertini [b], Simon Laflamme [a,f], Rafael Castro-Triguero [g]

[a] Department of Civil, Construction, and Environmental Engineering, Iowa State University, Ames, IA, USA
[b] Department of Civil and Environmental Engineering, University of Perugia, Perugia, Italy
[c] Department of Aerospace engineering, Iowa State University, Ames, IA, USA
[d] Department of Continuum Mechanics and Structural Analysis, University of Seville, Seville, Spain
[e] Department of Mechanical Engineering, Iowa State University, Ames, IA, USA
[f] Department of Electrical and Computer Engineering, Iowa State University, Ames, IA, USA
[g] Department of Mechanics, University of Cordoba, Campus de Rabanales, Cordoba, Spain

ARTICLE INFO

Article history:
Received 2 April 2017
Revised 6 July 2017
Accepted 8 July 2017

Keywords:
Structural health monitoring
Sensor network
Damage detection
Nanocomposite conductive concrete
Resistor mesh model
Damage localization
Smart concrete

ABSTRACT

Interest in self-sensing structural materials has grown in recent years due to their potential to enable continuous low-cost monitoring of next-generation smart-structures. The development of cement-based smart sensors appears particularly well suited for structural health monitoring due to their numerous possible field applications, ease of use, and long-term stability. Additionally, cement-based sensors offer a unique opportunity for monitoring of civil concrete structures because of their compatibility with new and existing infrastructure. In this paper, we propose the use of a computationally efficient resistor mesh model to detect, localize and quantify damage in structures constructed from conductive cement composites. The proposed approach is experimentally validated on non-reinforced and reinforced specimens made of nanocomposite cement paste doped with multi-walled carbon nanotubes under a variety of static loads and damage conditions. Results show that the proposed approach is capable of leveraging the strain-sensing and damage-sensitive properties of conductive cement composites for real-time distributed structural health monitoring of smart concrete structures, using simple and inexpensive electrical hardware and with very limited computational effort.

1. Introduction

Real-time condition assessment and structural health monitoring (SHM) of civil infrastructure can provide enhanced structural safety and increased maintenance service intervals through condition-based maintenance [1]. However, SHM is often complicated by the inherent size of the civil structures under monitoring and the inability of traditional sensors to distinguish between global (i.e. loss in stiffness) and local (e.g. a crack in grouted joint) properties [2]. For example, global vibration characteristics (e.g. modal frequencies and mode shapes) can be easily estimated from acceleration time histories through output-only operational modal analysis methods. However, correlating changes in modal parameters to localized damage cases has been shown more challenging [3,4].

For the deployment of real-time condition assessment strategies in civil infrastructure, the monitoring scheme must be capable of damage detection and localization [1]. A possible solution to the local-global damage localization challenge is the deployment of highly scalable sensing solutions to form dense sensor networks, deployed onto the structure's surface, that are capable of discretely monitoring local changes in a structure over its global area [5]. Various researchers have proposed dense sensor networks, often termed sensing skins, as a solution to the local-global challenge. Yao et al. [6] proposed large sensing sheets of resistive strain gauges (RSG) with embedded processors on a 50 μm thick polyimide sheet for crack detection and localization on civil infrastructure. Loh et al. [7] introduced a layer-by-layer assembled carbon nanotube nanocomposite sensing skin that, when combined with the electrical impedance tomography mapping technique, enabled two-dimensional damage detection. Hallaji et al. [8] developed a large-area sensing skin for damage detection in concrete structures, consisting of electrically conductive copper paint that is

* Corresponding author.
E-mail address: adowney2@iastate.edu (A. Downey).

http://dx.doi.org/10.1016/j.engstruct.2017.07.022
0141-0296/

applied to the surface of the concrete. Cracks in the underlying concrete resulted in a dislocation of the sensing skin, and, therefore, in a change in skin conductivity. Electrical impedance tomography was then used to detect and localize damage in the substrate. Downey et al. [9] proposed the use of a hybrid dense sensor network consisting of large-area strain-sensing capacitive-based sensors and RSGs for the low-cost monitoring of large structures. The various dense sensor networks presented here, while promising, lack the capability to directly detect a structure's internal damage. The problem of detecting internal damage is of great importance as, for instance, load bearing walls are often made of thick slabs of steel reinforced concrete composites and internal damage may not be evident on the surface. Other notable examples demonstrating the importance of detecting internal damage include the reinforced concrete beam-column joints that can undergo shear failure under seismic loading and grout failure in mechanically spliced column-footing connections [10].

A solution to the challenge of internal monitoring of civil structures is to embed self-sensing structural materials into the segments of interest to enable smart monitoring [11,12]. Self-sensing cement-based structural materials offer the benefit of easily binding with the monitored structure as they possess similar material properties as the structure being monitored [13]. Fabrication of self-sensing cementitious materials through the doping of carbon-based particles into traditional admixtures of cement has been achieved [14]. Various carbon-based materials have been mixed with cementitious materials, including carbon fibers [15,16], nano-carbon black [17] and, more recently, multi-walled carbon nanotubes (MWCNT) [4,18,19]. MWCNTs offer great potential due to their excellent electrical and mechanical properties [20,21]. For this reason, they have been employed in the fabrication of many strain sensing composite materials. It has been demonstrated that the cementitious material's strain sensing property is due to piezoresistivity caused by the slight pull-out of fibers passing through micro-cracks [16].

Research on damage detection and localization has been performed for various forms of conductive cement composites. Multiple examples of data-driven damage detection, where damage is inferred from a change in electrical signal [19,22,23], can be found in the literature. Chen et al. [15] demonstrated a data-driven damage detection approach in a carbon fiber-reinforced concrete beam under a three-point-bending test. The damage was clearly detected, but damage localization within the specimen was not achieved. Hou et al. [24] presented an electrical impedance tomography method for use with cementitious structures. Results demonstrated that the electrical impedance tomography method was capable of detecting and localizing damage in a polymeric fiber reinforced cementitious composite. However, repeated measurements were required along with various applied current distributions to solve the tomography mappings inverse problem. Furthermore, electrical impedance tomography requires the use of a finite element or finite difference method to obtain an approximation of the solution, because an analytical solution is generally difficult to formulate [25].

This work introduces a computationally efficient and direct model-based approach to damage detection, localization and quantification of crack type damage in self-sensing cement-based structural materials. Here, a simple resistor mesh model is created to approximate the self-sensing material. Varying strain and damage states can be introduced into the resistor mesh model through changing the resistive value of individual resistors. This capability is based on the hypothesis that the electrical resistivity of any self-sensing conductive material depends on its strain [18] and fault state (healthy/damaged) [26]. Cracks in the self-sensing material are considered to cause a reduction in conductivity since cracks are non-conducting when opened. The resistor mesh model is efficiently solved through nodal analysis, providing a voltage level for each model node, and compared to experimental data. Individual resistors within the model can then be adjusted to localize the damage within the material. This approach enables real-time detection and localization of damage in concrete structures with simple and inexpensive electrical hardware while requiring only light computations. The proposed method is validated for an MWCNT cement composite under static damage cases and a steel reinforced MWCNT cement composite under a four-point loading case. In the four-point loading case, a finite element analysis model is developed to update the resistor model with strain-induced resistance changes for each loading case.

The contributions of this paper are twofold: (1) a straightforward and easily solvable resistor mesh model is introduced and experimentally verified for damage detection, localization and quantification in multi-functional cement-based self-sensing materials; (2) experimental validation of the resistor mesh model for damage detection and localization in a steel reinforced cement-based beam is performed, successfully locating and detecting an internal damage case that is non-evident on the specimen's surface.

This paper is organized as follows. Section 2 presents background on the self-sensing cement-based material used for experimental validation, along with the biphasic DC measurement approach used for monitoring the self-sensing material. Section 3 presents the proposed resistor mesh model for damage detection and localization. Section 4 presents the three experimental validation cases and results. Section 5 concludes the paper.

2. Background

The self-sensing cement composite specimens used in this study are introduced in this section. Thereafter, the biphasic DC measurement approach used in the presented experiments is described, and its enhanced time stability in comparison to other existing methods is demonstrated along with its capability to monitor the strain sensitivity of the cement composites.

2.1. Self-sensing cementitious material

Specimens made of a self-sensing nanocomposite cement paste doped with MWCNT are used for model validation. Previously conducted axial compression tests have demonstrated that the MWCNT/cement-based matrix mix design considered here is capable of behaving as a strain-sensing structural material [18]. The fabrication process of the material and its sensing principle are described in details in Ref. [18]. Briefly, the composite is made by doping a traditional cementitious mixture with carbon nanotubes, providing the material with a piezoresistive strain sensing capability. Here, specimens were fabricated by adding 1% MWCNT (Arkema C100), with respect to the mass of cement, to deionized water and a surfactant (Lignosulfonic acid sodium salt). Nanotubes were dispersed in water by using a sonicator tip after a preliminary mechanical mixing. The obtained water-nanotube suspension was then mixed with type IV Portland cement. Four specimens were cast. The first into a $51 \times 51 \times 51$ mm^3 mold along with 4 stainless steel mesh electrodes (4×4 mesh, 1.2 mm wire diameter) for the strain sensing tests, as shown in Fig. 1. An additional 51 mm side cube, along with a $40 \times 40 \times 160$ mm^3 and a $100 \times 100 \times 500$ mm^3 beam were cast for experimental model validation. These three samples will be discussed later.

The use of any strain-sensing material requires the assumption of an electromechanical model to relate strain to a measurable electrical parameter. While various equivalent electromechanical models for cement-based materials doped with MWCNT have been

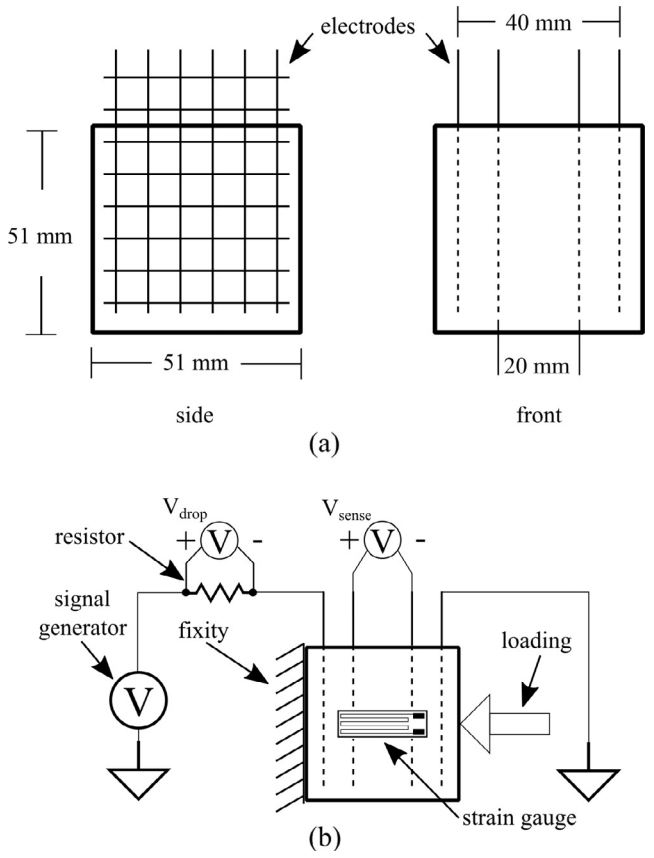

Fig. 1. Self-sensing structural material specimen consisting of MWCNTs suspended in a cement matrix used for strain sensitivity testing: (a) specimen dimensions; (b) experimental setup for validation of the materials strain-sensing capability.

introduced [27,28], these models typically conclude that only resistance is influenced by the mechanical deformation [28]. Under this assumption, the resistance-strain relationship can be presented as:

$$\frac{\Delta R}{R} = -\lambda\varepsilon \tag{1}$$

where R is the specimen's unstrained nominal resistance, ΔR is the incremental variation in electrical resistance caused by the axial strain, λ is the material's gauge factor and ε is the strain assumed positive in compression. According to the simplified model presented in Eq. (1), λ is the only parameter characterizing the strain-sensitivity of the material.

2.2. Biphasic DC measurement approach

Self-sensing cement-based materials doped with carbon nano inclusions are known to exhibit an inherent time-based drift in their electrical output. When using a DC measurement technique, this drift usually represents itself as an increase in the resistance starting from the time the sensing current is applied. The drift can be recognized in various research and is often attributed to material polarization [29,30], variations in material's dielectric constant [31] or direct piezoelectric effect [32]. Various techniques for minimizing the effect of this drift have been proposed, including: comparing a sensing material with a control sample [33], delaying measurements until the drift levels out [34] and using AC measurements techniques [26].

This work is aimed at detecting, localizing and quantifying cracks in reinforced self-sensing concrete structures by exploiting permanent local changes in electrical resistance induced by the cracks. To do so, resistance measurements made using a standard DC measurement method were found to be inappropriate, due to the constantly changing resistance caused by material polarization. Similarly, AC measurements made with an LCR were also deemed unacceptable due to the need to simultaneously monitor various sections of a continuous structure such as a beam. In order to overcome the limitations of existing DC and AC measurement methods, this work utilizes a biphasic DC measurement approach able to provide consistent and stable long-term results by continuously charging and discharging the self-sensing material, also allowing multi-section readings. The method has been proposed by the authors and is the focus of a separate work [35]. Its main features are introduced here for completeness.

In the biphasic DC measurement method, the biphasic signal is sourced from a function generator producing a 2 Hz square wave ranging from −2.5 to 2.5 V across the specimen with a duty cycle of 50%. The applied sensing current is presented in Fig. 2(a), and is labeled as $V_{applied}$. Material depolarization is obtained during the sensing current's discharge region and DC measurements are taken during the measurement region of the square wave. DC voltage measurements are taken 0.2 s after the start of the periodic square wave measure cycle, as shown in Fig. 2(a). Resistance, R, is calculated by dividing the measured voltage, V_{sense}, by the current, i, flowing through the specimen cross-section, as follows:

$$R = \frac{V_{sense}}{i} \tag{2}$$

The current, i, in Eq. (2), is obtained by monitoring the voltage drop, V_{drop}, across a resistor, $R_{in-line}$, set in series with the test specimen, namely

$$i = \frac{V_{drop}}{R_{in-line}} \tag{3}$$

The voltage and, therefore, the resistance, can be sampled at multiple points along a continuous beam. This way, the biphasic DC measurement approach allows for the simultaneous measurement of every section in a multi-sectioned test specimen. In addition to the applied voltage, Fig. 2(a) also presents the voltage drop across the in-line resistor (V_{drop}) and the four-probe sense voltage (V_{sense}), where the sense voltage is sampled as shown in Fig. 1(b).

The capability of the biphasic DC measurement approach to eliminate resistance drift caused by material polarization is demonstrated in Fig. 2(b). In this plot, the resistance of the specimen presented in Fig. 1 is shown using both a traditional DC measurement and the biphasic DC measurement approaches for the first 300 s after a sensing current is applied to the sample. A four-probe configuration is used to eliminate the effects of contact resistance [36]. Resistance results obtained using DC measurement experiences an increasing drift with respect to time. The drift is greater in the first few seconds after the sensing current is applied, while it tends to decrease afterward. In comparison, the proposed biphasic DC measurement technique provides a constant resistance measurement with no polarization drift present in the first 300 s. It is hypothesized that the discharge region of the periodic square wave acts to fully discharge the sensor between subsequent measure regions. The smaller resistance value measured through the biphasic DC approach in comparison to the result of the standard DC method can be explained by the circumstance that the biphasic approach limits polarization time to 0.2 s, thus also limiting the related apparent increase in resistance.

2.3. Strain sensing characterization

The capability of the biphasic measurement to be used for strain-sensing in smart structural materials is demonstrated in

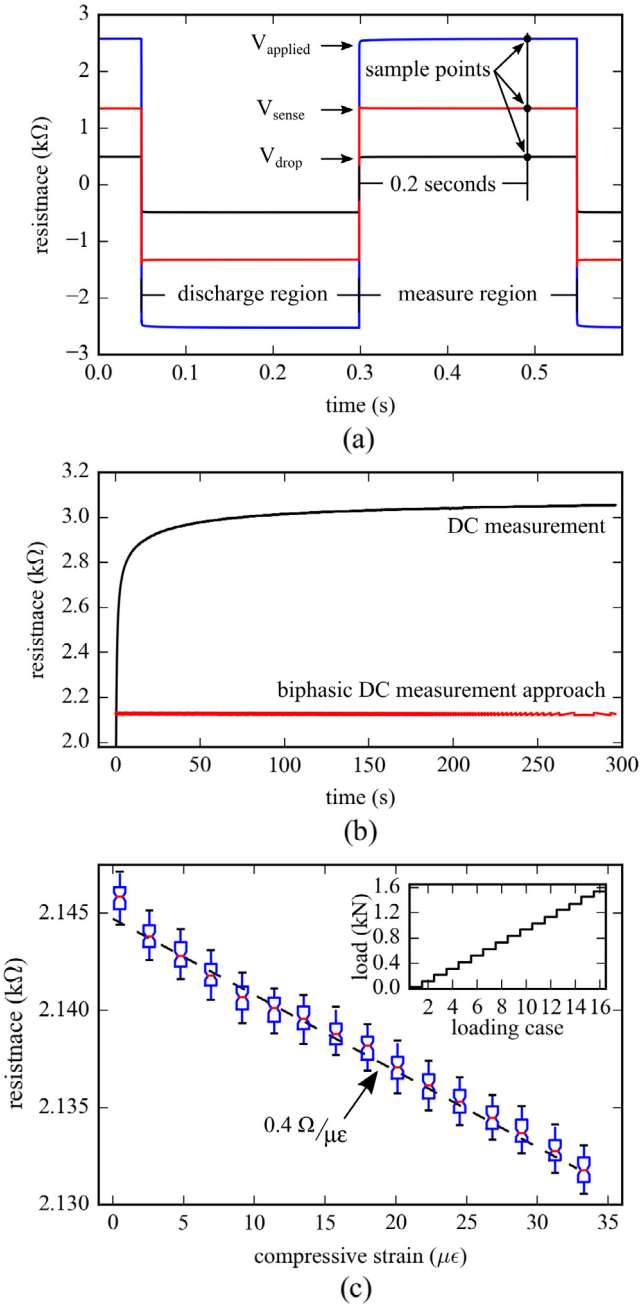

Fig. 2. Biphasic DC measurement approach: (a) voltage signals for a 2 Hz square wave sensing current; (b) comparison of DC four-probe resistance measurement vs the biphasic DC measurement approach; (c) strain sensitivity for the specimen shown in Fig. 1.

Fig. 2(c). The nanocomposite cement paste cube presented in Fig. 1 is tested in a quasi-static compressive loading test. The load is applied in 0.1 kN step increments from fully unloaded to 1.5 kN. The loading time history is shown in the insert in Fig. 2(c). Seventy-five resistance samples were taken at 2 samples per second (S/s) for every loading step and are presented as a series of box plots to show the sample distribution. Resistance values are calculated using Eq. (2) as presented above. Strain is concurrently measured with RSGs adhered to opposite sides of the specimen. A linear regression of the data is performed and a linear relationship between the measured strain and resistance with a sensitivity of 0.4 $\Omega/\mu\varepsilon$ was obtained. This strain sensitivity was found to agree well with the experimental data acquired during testing of specimen III, the only specimen to undergo a strain-induced changen in resistance. However, the effect of scaling and normalizing the strain sensitivity value will need to be addressed in future work. For the purpose of this introductory work, the strain sensitivity value is assumed valid and used throughout the rest of the work and adjusted to electrical resistivity where appropriate. The maximum loading case for specimen I was limited to 1.5 kN, corresponding to 34 $\mu\varepsilon$, due to the testing apparatus. During testing of specimen III a maximum compression of 65 $\mu\varepsilon$ was recorded with an externally mounted strain gauge. The linearity of strain sensitivity for compressive loading has been documented well passed this loading level and is assumed to remain linear for the purpose of this study [17,19,37,38]. As expected, the specimen resistance decreases with the increasing compressive force. This decrease in resistance stems from the reduction in the average distance among MWCNTs, therefore decreasing the resistance of the conductive networks through the quantum tunneling effect. This same theoretical approach applies in tension, where the difference in gauge factors is small enough that a common gauge factor can be assumed [39]. For concrete specimens in tension, this theoretical approach governs until the opening of micro-cracks starts to control the conductive networks, however, for simplicity micro-cracks are not modeled in this work. The piezoresistive effect described here has been demonstrated under multi-axial strain [40].

3. Resistor mesh model

This section introduces the proposed resistor mesh model for damage detection, localization and quantification in conductive cement-based composites. First, the resistor mesh model and its methodology are proposed. Then, a validation scheme and the specimens used for model validation are presented.

3.1. Methodology

The resistor mesh model shown in Fig. 3 is a simplified form of the resistor mesh model proposed here for the detection, localization and quantification of damage in conductive cement-based composites. A rectangular mesh is first constructed to mimic the geometry of the conductive specimen, whereby it is noted that this

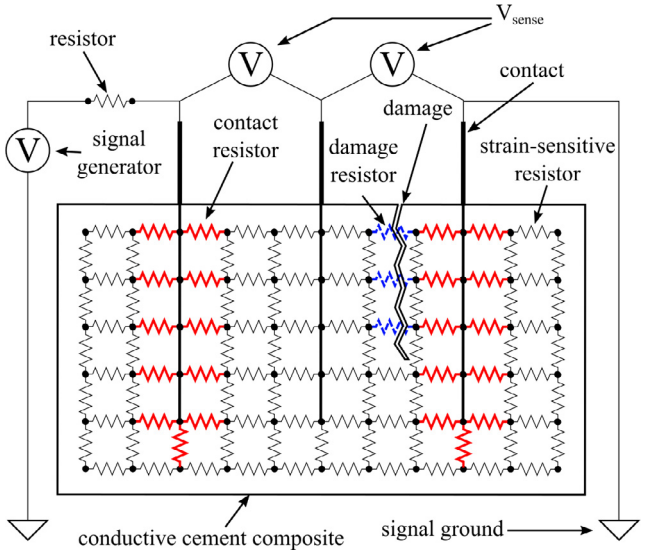

Fig. 3. A resistor mesh model with a 10×5 resistor mesh for crack detection, localization and quantification in cement composite structures with key components highlighted.

work focuses exclusively on the construction of 2-D rectangular resistor meshes. The use of 3-D meshes of varying shapes would not entail any substantial change in the methodology. However, this topic is beyond the scope of this introductory work. Contacts are introduced into the model as non-resistive elements between model nodes. Voltage measurements are made as the differential sensing voltage between contacts as diagrammed in Fig. 3. The introduction of three resistor types into the resistor mesh model are considered: (i) strain-sensitive resistors, (ii) contact resistors and (iii) damage resistors. The model's capability to detect, localize and quantify damage is based on the hypothesis that a resistor mesh model, with the correct consideration of resistor type and placement, is capable of accurately accounting for the conductive cement-based composites strain and damage state over the full geometric shape considered in the model. An explanation of the resistor types is presented in what follows.

Strain-sensitive resistors, represented by light continuous lines in Fig. 3, make up the majority of the resistor-mesh model. Their values are adjusted through the use of a finite element analysis (FEA) model to estimate strains present in the model and the material's known strain sensitivity. Their nominal values are determined considering the contact resistance through matching the current flow and voltage measurements of the specimen under study to those obtained from the resistor mesh model. Their value is, therefore, dependent on the density of the resistor mesh used and may not be directly related to material properties. In cases where the strain is considered to be non-relevant to the detection of damage, strain-sensitive resistors may be left as their nominal resistance values, therefore removing the need to develop a separate FEA model.

Contact resistors, represented by thick continuous line resistors in Fig. 3, are added to account for the increased resistance at the current carrying contacts caused by the electrochemical reaction between the conductive cement structure and metal electrodes. For cement composites with carbon-based additives, the value of the contact resistance may be considerable [36,41]. Here, contact resistors are added only where one resistor extremity is in direct contact with the embedded electrode and the opposite resistor extremity interacts with the resistor mesh. The contact resistance is fully accounted for at the cement/contact interface, as demonstrated by Han et al. [41]. The value of the contact resistance is set through monitoring the experimental data and are adjusted together with the resistance value of strain-sensitive resistors.

Damage resistors, represented by dashed blue resistors in Fig. 3, introduce damage into the model at locations of observed cracking or through appropriate selection to reconstruct an experimental measurement. Here, cracks in the self-sensing material are considered to cause a strong reduction in conductivity, because cracks may be non-conducting when opened. Damage resistors are replaced with non-conductive elements in the model. In some cases, the use of damage resistors that maintain some level of conductivity may be appropriate. This strategy is beyond the scope of this work.

The correctly assembled resistor mesh model can be solved for each unknown voltage as a system of linear algebraic equations. This nodal analysis problem only requires $V_{applied}$ as a model input. The model's calculated current flow and voltage at contact locations can then be used for comparison with experimental values. In this work, a 2-D resistor mesh is used for modeling the experimental specimens, assuming a constant cross-section. This simplification allows for the modeling of the embedded contact mesh as a single linear contact through the depth of the material. The effects of contact selection and placement on electrical field distribution in the material and optimal contact placement for damage detection will need to be addressed in future works. Here, the resistor models used to reproduce the experiments are solved in SPICE [42], an open source analog electronic circuit simulator.

3.2. Model validation

Experimental validation of the resistor mesh model is conducted using three self-sensing cement composites doped with MWCNTs (denoted as specimen I, II and III). Specimen I is designed to validate the simple case of a controlled damage induced into a non-reinforced conductive cement beam without strain-induced resistance changes. Specimen II is designed to validate the damage detection model for induced damage in a cubic specimen, where edge effects are considered to be the greatest among the three specimens. Additionally, the low number of contacts used in this case demonstrates the resistor model's capability to function even without dense networks of electrodes. Again, no strain-induced resistance change are considered for specimen II. Specimen III is designed to validate the resistor mesh model for damage detection, localization and quantification in a steel reinforced conductive cement beam under a four-point loading condition. An FEA model is used to update strain-sensitive resistors in the model. During loading, an uncontrolled damage develops in a pre-existing surface crack on the left-most contact. Model parameters and material properties of the specimens are presented in Table 1.

For validation purposes, the experimental data, locations of known damage (induced or observed) and FEA models (specimen III only) are used to construct a resistor mesh model that is then solved using SPICE. The model's output is compared to experimental data and the results are reported, as diagrammed in Fig. 4. Voltage measurements are acquired using the biphasic DC measurement approach presented in Section 2. Results from the resistor mesh model and experimental results are presented as voltage drops between sections.

4. Experimental validation and discussion

The experimental setup, results and discussion for each specimen are presented in this section.

Table 1
Specimens fabricated for validation.

	Specimen		
	I	II	III
Dimensions (h × w × d (mm))	40 × 40 × 160	51 × 51 × 51	100 × 100 × 500
Number of contacts	8	5	16
Contacts depth (mm)	35	49	60
Resistor mesh model (h × d)	40 × 160	51 × 51	50 × 250
Circuit nodes	6401	2602	3126
Total solve time (s)	3.29	0.37	14.70
Nominal resistance (Ω)	500	1000	105
Contact resistance (kΩ)	44	80/37 (L/R)	10.5
Current flow (mA)	0.709	0.903	2
Applied voltage (V)	2.5	2.5	2.5

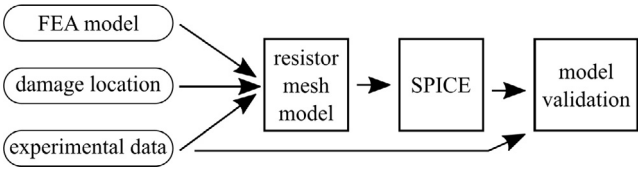

Fig. 4. Validation scheme for the proposed resistor mesh model.

4.1. Specimen I: eight contact beam

Specimen I consisted of an eight contact (seven sections) non-reinforced cement composite beam intended to validate the resistor mesh model in a simplified form. Fig. 5 diagrams the experimental setup for the beam, consisting of monitoring the voltage drop over all seven sections and inducing a controlled damage into the center of Section 4. Damage was introduced in the form of a 1 mm wide crack (cut), using a hacksaw. Cuts were made in 5 mm steps from 0 to 30 mm with voltage measurements made starting from the healthy state and after each cut.

A resistor mesh model of 40 × 160 resistors was generated to approximate the specimen. The model was then calibrated to the experimental data through the adjustment of the resistance values for the strain-sensing and contact resistor values to match the specimen's experimentally obtained current flow and voltages for the beam's healthy state as shown in Fig. 6(a). The voltage drops over Sections 3 and 5 were found to be greater than what would be expected for an undamaged section. Upon inspection, surface cracks were found to be present in these sections (see Fig. 5(c)) and were added as pre-existing damages to the resistor mesh model as denoted in Fig. 5(a). Crack 1, as labeled in Fig. 5(a) was added as a 12 mm crack from the surface down in the center of Section 3, while crack 2 was added as an 8 mm crack from the surface down in the center of Section 5. Both cracks were visible on the front, top, and back of the beam and are assumed to have propagated through the beam. Fig. 6 reports the results for both resistor mesh model (labeled model) and the corrected resistor mesh model (labeled corrected model) that accounts for the pre-existing cracks. Damage is introduced into the resistor mesh model in 5 mm steps.

Results presented in Fig. 6(a) demonstrate that the resistor mesh model is capable of reconstructing the electrical characteristics of the beam in both its corrected and uncorrected forms. Moreover, the results for the fully damaged beam (30 mm cut), presented in Fig. 6(b), show that the model is capable of detecting and localizing the damage as occurring in Section 4. Also, it is shown that the model is capable of accurately tracking the damage as it propagates deeper into the section (Fig. 6(c)). As the crack depth increases, the specimen's sensitivity to damage grows. This was expected as each unit increase in crack depth produces a larger

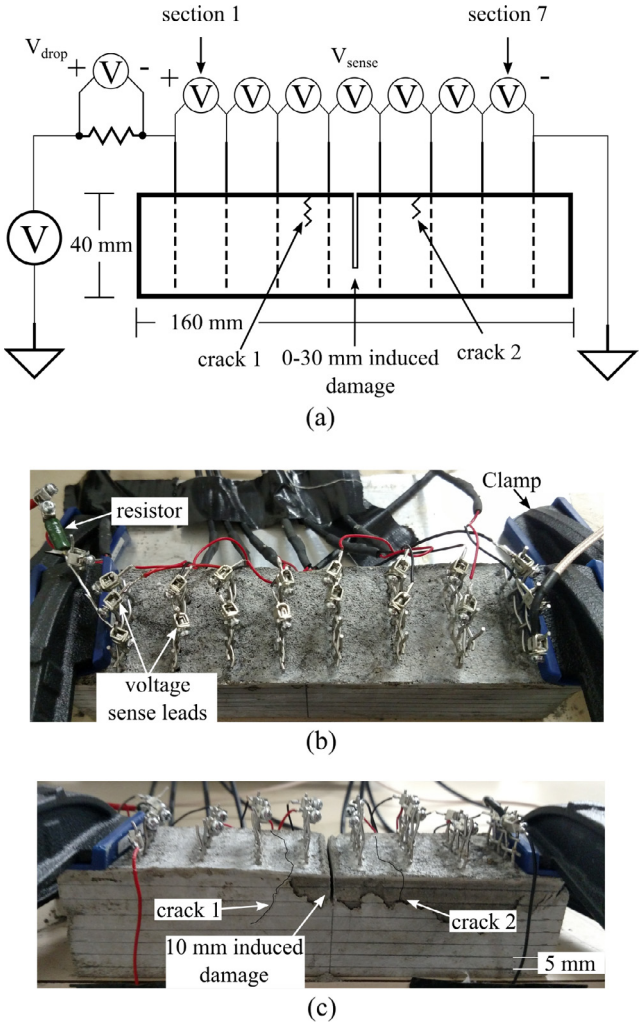

Fig. 5. Experimental setup for specimen I, showing: (a) experimental setup with modeled locations for the pre-existing damage (crack 1 and 2) and the induced damage; (b) experimental wiring; (c) pre-existing damage cases and an induced damage of 10 mm.

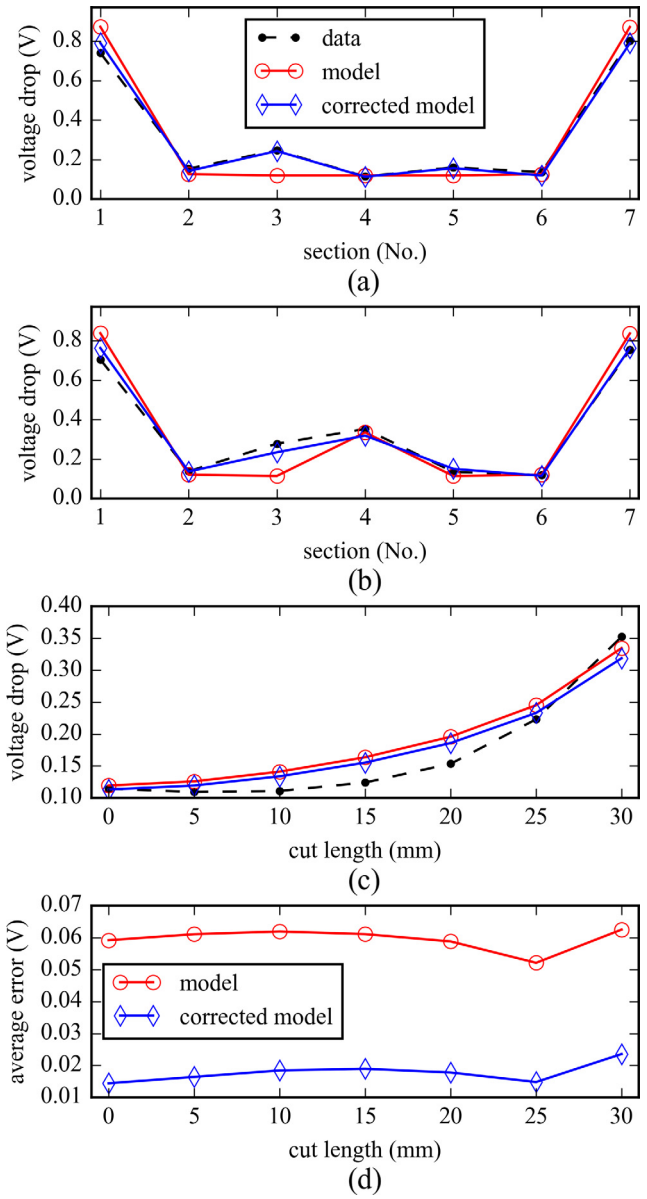

Fig. 6. Experimental data and analytical model results for specimen I, showing: (a) healthy state; (b) 30 mm center cut; (c) voltage drop for Section 4; (d) average total error for all sections.

relative change in the conductive area across the cross-section of the beam. The resistor mesh model, in both its uncorrected and corrected forms, is capable of replicating this increase in sensitivity as shown in Fig. 6(c). Lastly, the average error of all the sections as a function of the induced crack length is presented in Fig. 6(d) for both the uncorrected and corrected model. As expected, the uncorrected model displays a higher average error across all crack lengths due to lack of knowledge about the pre-existing cracks. Overall, the error is relatively constant for both model cases over the range of the induced crack length. This demonstrates that the simplified 2-D resistor mesh model is capable of tracking the damage case to a degree of certainty.

4.2. Specimen II: five contact beam

Specimen II consisted of a five contact (four sections) self-sensing non-reinforced cement paste cube intended to validate the resistor mesh model for use in a highly compact specimen that is subject to a large amount of edge effects, in a simplified form. Fig. 7 diagrams the experimental setup for the cube, consisting of monitoring the voltage drop over all four sections and inducing a controlled damage into the center of Section 2. Again, damage was added using a hacksaw and cuts were made in 5 mm steps from 0 to 25 mm. At 25 mm, an embedded contact was hit by the hacksaw blade. Therefore, the damage cases were not continued past 25 mm.

A resistor mesh model of 51×51 resistors was developed to model the specimen. As before, the model was calibrated to the experimental data through the adjustment of the resistance values for the strain-sensing and contact resistor values to match the specimen's experimental current flow and voltage drops. These results are presented in Fig. 8(a) for the healthy case. In specimen II the voltage drop in Section 1 was found to be higher than the voltage drop in Section 4. However, upon inspection, no visible surface damage was found on any face of the sample. Therefore, the cause for this discrepancy was hypothesized to be a difference in the average contact resistance of the two outside contacts, possibly caused by a local variability of the material. A corrected model was developed to accommodate for this change in contact resistance with a contact resistance of 80 Ω being used for the contact on the left and a contact resistance of 37 Ω being used on the right. Results are presented in Fig. 8 for both the uncorrected model

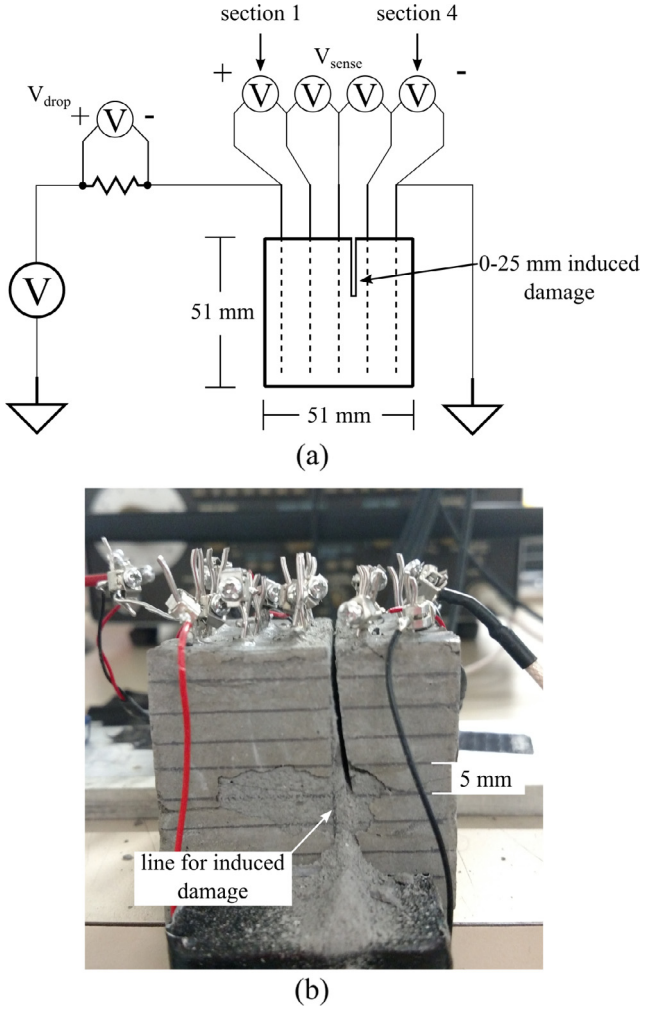

Fig. 7. Experimental setup for specimen II, showing: (a) experimental setup; (b) induced damage of 25 mm.

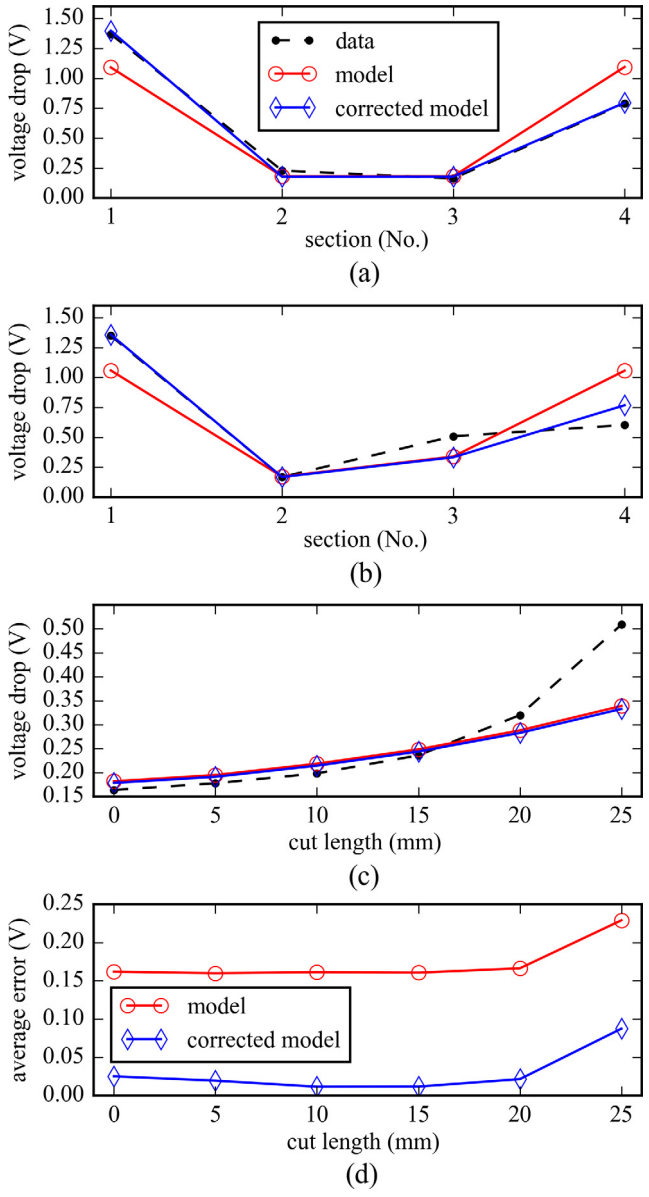

Fig. 8. Experimental data and analytical model results for specimen II, showing: (a) healthy state; (b) 25 mm center cut; (c) voltage drop for Section 3; (d) average total error for all sections.

(using a contact resistance of 58 Ω on both sides) and the corrected model.

Similar to results obtained from Specimen I, results presented in Fig. 8(a) demonstrate that the resistor mesh model is capable of reconstructing the electrical characteristics of the cube specimen in both its corrected and uncorrected forms. The capability of the model to account for varying contact resistance values further enhances the capability of the resistor mesh model for damage detection. Results for the fully damaged beam condition (25 mm cut) are presented in Fig. 8(b). The disagreement between the models and experimental data for Sections 3 and 4 for the 25 mm damage case is assumed to be a function of the saw contacting the embedded contact. This assumption is further strengthened by the changing voltage drop (Fig. 8(c)) for Section 3 as a function of the induced crack length. It can be seen that both the corrected and uncorrected models are capable of tracking the damage growth up to the 20 mm crack length. However, the 25 mm crack length shows a significant level of disagreement between the model and the experimental data. Lastly, the average error of all the sections as a function of the induced crack length is presented in Fig. 8(d). The uncorrected model displays a higher average error across all crack lengths but both models retain a relatively constant error over all induced damage cases except for the final damage case, as expected.

4.3. Specimen III: sixteen contact beam

Specimen III is a steel reinforced cement paste beam with 16 embedded contacts (15 sections), intended to validate the model's capability to fully detect, localize and quantify damage in an uncontrolled damage case in the presence of steel reinforcement. The beam is presented in Fig. 9, where Fig. 9(a) annotates the key components of the beam and Fig. 9(b) is a picture of the experimental setup. Damage present on the top extremities of the beam in Fig. 9(b) occurred while extracting the beam from the molds. The surface of the beam contained multiple cracks, and these were photographed to enable crack monitoring during testing. Six RSGs were adhered onto the face of the beam and were used for validating the FEA model built for updating strain-sensitive resistors. Twenty-four loading steps were applied in 0.1 kN intervals. The load cell in Fig. 9(b) was used to evenly distribute the loading onto the two steel pins. The beam suffered damage during the

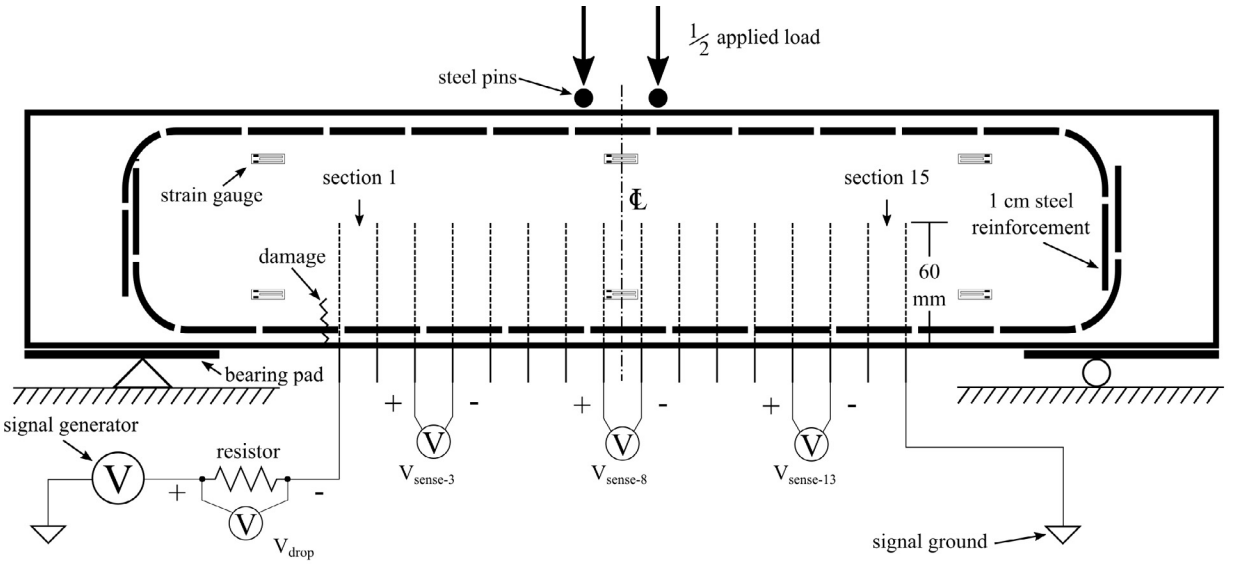

(a)

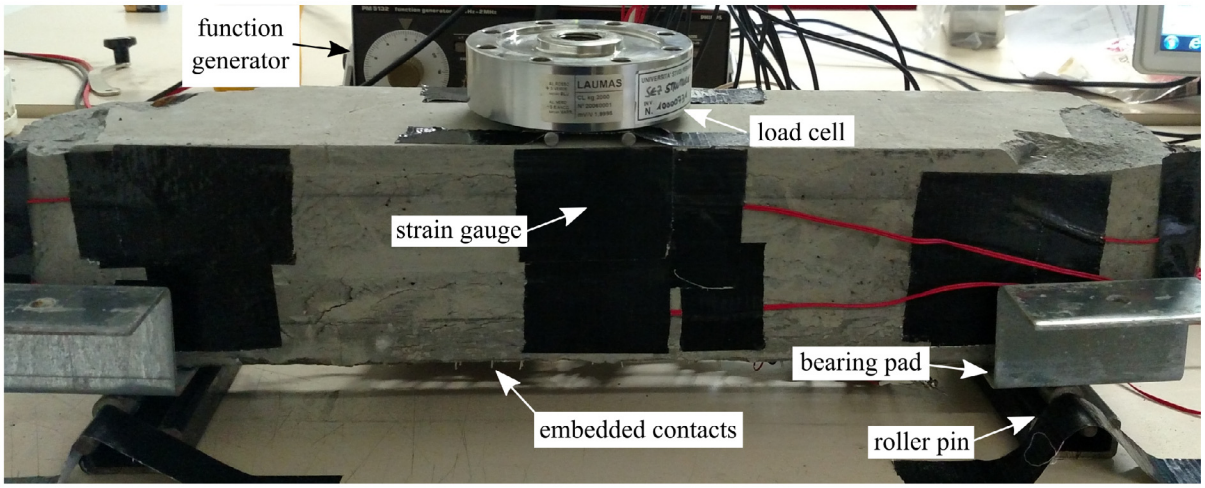

(b)

Fig. 9. Experimental setup for the self-sensing reinforced cement paste beam: (a) annotated diagram labeling key components of the test setup; (b) experimental setup as tested, (with the load bearing clamp removed for clarity).

application of the 1.8 and 1.9 kN loads. An audible crack was heard during the application of both loading cases. Experimental results presented later in this section and the resistor mesh model strongly suggest that the damage occurred on the outside of the left-most monitored section, as annotated in Fig. 9(a). This damage case demonstrates the capability of the resistor mesh model to detect, localize and quantify damage in a steel reinforced cement composite beam. A resistor mesh model of 50×250 resistors was used to model the specimen as it provided accurate analytical results while requiring a relatively short computation time.

The FEA model for updating the strain-sensitive resistors consisted of 50,000 eight-node solid elements and developed using Abaqus [43]. The steel reinforcements were incorporated into the 3-D FEA model. The front surface of the FEA solved strain map is shown in Fig. 10. Four of the sixteen embedded contacts were added to the FEA model, the remaining contacts were withheld due to the software imposed limitation of 50,000 elements. The FEA model was validated using the RSGs diagrammed in Fig. 9(a). A 2-D strain map was developed from a cross section taken from the center of the 3-D strain map. The 2-D strain map was used to update the resistor mesh model using a strain sensitivity of $0.4\ \Omega/\mu\epsilon$.

The experimental results and the resistor mesh model are presented in Fig. 11. As shown in the figure, the experimental data shows a significantly large voltage drop over a few adjacent sections located in the middle of the specimen. This deviation is assumed to be a function of the cracks present in the specimen and a slight cavity in the top of the beam that formed during casting and extends through Sections 6, 7 and 8. These irregularities were due to the decrease in workability of the carbon-doped cement paste and difficulties in getting the cement to flow around the densely packed electrodes. However, due to the high number of surface cracks, the cavity in the cement paste and the circumstance that damage formed outside this region, it was not necessary to develop a corrected model for specimen III.

As stated before, the beam experienced damage during the application of the 1.8 kN load that produced an audible crack.

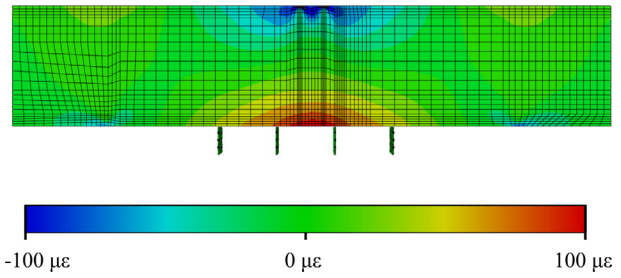

Fig. 10. FEA model results (strain) of specimen III used for developing strain fields used in the implementation of the resistor mesh model.

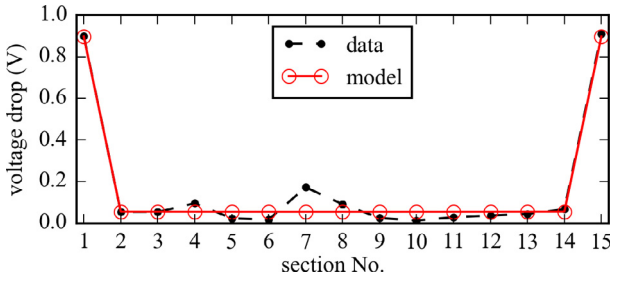

Fig. 11. Experimental analytical model results for the healthy state of specimen III.

The results shown in Fig. 12(a) allow for a data-driven approach to damage detection and localization. First, the change in voltage for Section 8 (the center section) is inspected. As the loading increases, the voltage drop across the center section increased as a consequence of an increase in the section's electrical resistance. This increase in voltage drop is related to tension forming along the bottom of the beam (Fig. 10), and reaches a maximum around 1.4 kN. Thereafter, any increase in tension along the bottom of the beam does not cause an increase in the voltage drop as the material starts to form excessive amounts of micro-cracks and looses its sensitivity to strain [16]. Moving outward from the center in symmetric pairs, each pair of sections demonstrated a constant and matching change in voltage drop over all the sections. This was expected due to the symmetric loading of the beam and is demonstrated by the paired Sections 4 & 12 and Sections 6 & 10, shown in Fig. 12(a). Other sections are not shown for clarity.

Constant and steady change in a section's electrical resistance and, therefore, its voltage drop, is caused by the material's strain-sensing capability [22]. In comparison, an abrupt increase in resistance can be easily correlated to a damage case caused by material failure [19]. Such an abrupt increase in resistance can be recognized as a sudden increase in voltage drop, as shown in Fig. 12(a) for Section 1. The corresponding decrease in the voltage drop of Section 15 is a reaction to the increase in the voltage drop in Section 1. Upon closer inspection and by a comparison with pictures taken of the undamaged beam, no visible lengthening of any of the surface cracks were observed. Instead, based on the audible cracking noise heard at that stage of loading and based on the experimental data and its comparison with the predictions of the resistor mesh model, it was concluded that internal damage occurred on the outside of the left-most contact, most likely due to a shear failure through the surface crack presented in Fig. 12 (b) and (d). Additionally, upon further testing until complete failure [23], the beam was found to fail through the same surface crack with a maximum loading of 113 kN. Through further inspection of the data, it can be noted that the voltage drop across Section 15 decreases after the application of the 1.6 kN step, prior to the audible crack being heard during the application of 1.8 kN. Upon inspection of the entire data set, it was noted that a majority of the sections exhibited an increase in voltage drops. However, because this increase is low and distributed across most of the sections, it is difficult to attribute the causes of this redistribution of voltage drops. In comparison, the voltage variation during the 1.8 kN step is clear and distinct, allowing for the localization of damage. Damage may have been detected earlier using more advanced algorithms.

Here a data-driven approach is used to match the individual elements of the resistor mesh model to the experimental data available (e.g. voltage drops, audible cracks and external cracks). The development of algorithms for the placement of damaged resistor nodes within a complex structure, such as the beam currently under consideration, are needed to facilitate automated damage detection in structures using the proposed method. The resistor mesh model's capability to detect and localize damage for specimen III are presented in Fig. 12(c). The model's steady and mostly linear increase in Section 1 & 15's voltage drop is caused by the strain-sensitivity of the material, as estimated by the FEA model. This increase in the voltage drop relates to an increase in the section's average resistance, and shows a strong agreement with the experimental data (i.e. by comparing results in Fig. 12(a) and (c)). The abrupt increase that occurs during the application of 1.8 and 1.9 kN is a result of a crack-induced damage that occurred at the left-most contact. To reproduce this crack, damage-type resistors were introduced into the resistor mesh model. Cracks were added to the contact resistor element on the outside of the resistor mesh model. First, a resistor replicating a

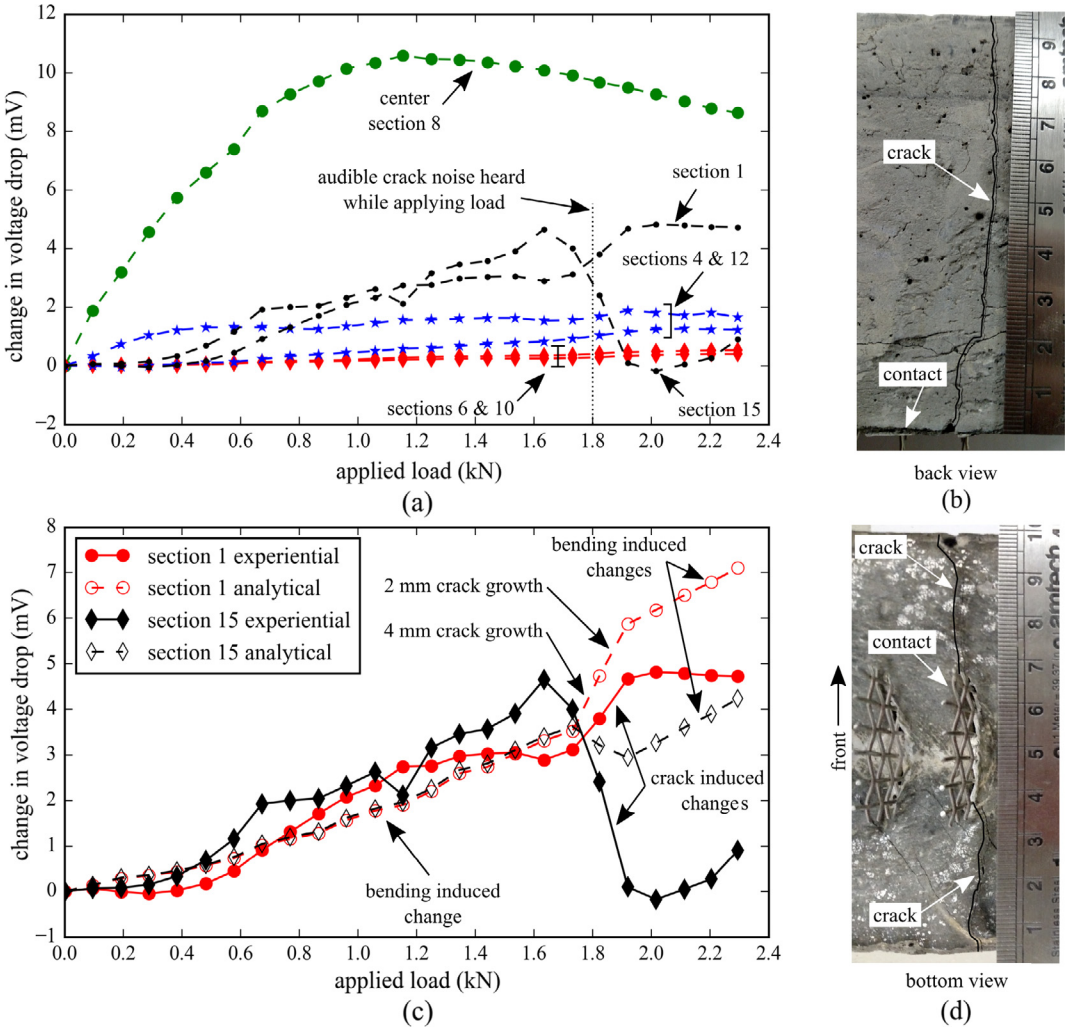

Fig. 12. Experimental data and analytical model results for specimen III, showing: (a) measured change in voltage drop as a function of the applied load; (b) crack detected outside Section 1; (c) analytical model versus experimental results for voltage drop measured at Section 1; (d) bottom view of the surface crack on the outside of Section 1.

4 mm crack was added into the resistor mesh model on the outside of the left-most contact, as shown in Fig. 9(a), to account for the pre-existing crack. Thereafter, a 4 mm crack was added during damage case associated with 1.8 kN. Next, due to the decrease in sensitivity as the cracks move further into the beam, a 2 mm crack was added during damage case associated with 1.9 kN. These cracks resulted in a total simulated crack length of 10 mm. The introduction of these cracks into the resistor mesh model was found to accurately match the experimental data and is useful in verifying that the damage case is present on the outside of the left most sensor. Ultimately, this beam was found to fail at the left most contact, further supporting our conclusion drawn here [23]. The successful damage identification, localization, and quantification in the reinforced cement paste beam shows that the resistor mesh model could be used in presence of a limited amount of steel reinforcement. It is hypothesized that the contact resistance present at the interface between the cement composite and steel reinforcement prevents the majority of the sensing current from passing through the steel reinforcement. The effects of highly conductive reinforcement in conductive cement composites is an area of future study. Alternatively, a segment of conductive concrete could be embedded in a beam of traditional (i.e. highly resistive) concrete, as presented in Ref. [13], to further isolate the highly conductive steel reinforcement.

5. Conclusion

This work introduced a resistor mesh model capable of damage detection, localization and quantification within structural elements made of non-reinforced and reinforced conductive and strain-sensing cement composites, using electrical outputs measured from the material. Based on an equivalent mesh of three different types of resistors, the proposed method is capable of reproducing the electrical response of structural elements fully or partly made of smart concrete. In particular, it allows to accurately reproduce strain-induced and damage-induced changes in voltage drops across multiple sections under the application of biphasic DC electrical inputs. The proposed method is validated through a campaign of experimental tests on three specimens made of nanocomposite cement paste doped with MWCNT, a smart composite material that is known to exhibit strain-induced changes in electrical resistivity under application of a mechanical loading. More specifically, two non-reinforced specimens were tested under controlled damage cases, while a steel reinforced MWCNT-cement paste composite beam was tested under a four-point loading case with an uncontrolled damage pattern. In the four-point loading case, a finite element analysis model was developed to update the resistor model with strain-induced resistance changes for each loading case.

The results demonstrated that the proposed approach successfully anticipates the electrical response of smart concrete structural elements and enables real-time detection, localization and quantification of crack-type damage with very simple and inexpensive electrical hardware and a limited computational cost. Future work includes the expansion of the proposed resistor mesh model into the third dimension, development of algorithms for the placement of damaged resistor nodes into a 3-D resistor mesh model and studying the effects of highly conductive reinforcement in conductive cement composites.

Acknowledgment

The support of the Italian Ministry of Education, University and Research (MIUR) through the funded Project of Relevant National Interest (PRIN) entitled "SMART-BRICK: Novel strain-sensing nano-composite clay brick enabling self-monitoring masonry structures" (protocol No. 2015MS5L27) is gratefully acknowledged. This work is also partly supported by the National Science Foundation Grant No. 1069283, which supports the activities of the Integrative Graduate Education and Research Traineeship (IGERT) in Wind Energy Science, Engineering and Policy (WESEP) at Iowa State University. Their support is gratefully acknowledged. This work was also partly supported by the Ministerio de Economía y Competitividad of Spain and the Consejería de Economía, Innovación, Ciencia y Empleo of Andalucía (Spain) under projects DPI2014-53947-R and P12-TEP-2546. E. G-M was also supported by a FPU contract-fellowship from the Spanish Ministry of Education Ref: FPU13/04892.

References

[1] Farrar CR, Lieven NAJ. Damage prognosis: the future of structural health monitoring. Philos Trans Roy Soc A: Math Phys Eng Sci 2007;365 (1851):623–32. http://dx.doi.org/10.1098/rsta.2006.1927. URL https://doi.org/10.1098%2Frsta.2006.1927 .

[2] Ubertini F, Comanducci G, Cavalagli N. Vibration-based structural health monitoring of a historic bell-tower using output-only measurements and multivariate statistical analysis. Struct Health Monit 2016;15(4):438–57. http://dx.doi.org/10.1177/1475921716643948. URL https://doi.org/10.1177%2F1475921716643948.

[3] Alvandi A, Cremona C. Assessment of vibration-based damage identification techniques. J Sound Vib 2006;292(1–2):179–202. http://dx.doi.org/10.1016/j.jsv.2005.07.036. URL https://doi.org/10.1016%2Fj.jsv.2005.07.036 .

[4] Ubertini F, Materazzi AL, D'Alessandro A, Laflamme S. Natural frequencies identification of a reinforced concrete beam using carbon nanotube cement-based sensors. Eng Struct 2014;60:265–75. http://dx.doi.org/10.1016/j.engstruct.2013.12.036. URL https://doi.org/10.1016%2Fj.engstruct.2013.12.036 .

[5] Flatau A, Chong K. Dynamic smart material and structural systems. Eng Struct 2002;24(3):261–70. http://dx.doi.org/10.1016/s0141-0296(01)00093-1. URL https://doi.org/10.1016%2Fs0141-0296%2801%2900093-1 .

[6] Yao Y, Glisic B. Detection of steel fatigue cracks with strain sensing sheets based on large area electronics. Sensors 2015;15(4):8088–108. http://dx.doi.org/10.3390/s150408088. URL https://doi.org/10.3390%2Fs150408088 .

[7] Loh KJ, Hou T-C, Lynch JP, Kotov NA. Carbon nanotube sensing skins for spatial strain and impact damage identification. J Nondestr Eval 2009;28(1):9–25. http://dx.doi.org/10.1007/s10921-009-0043-y. URL https://doi.org/10.1007%2Fs10921-009-0043-y .

[8] Hallaji M, Seppänen A, Pour-Ghaz M. Electrical impedance tomography-based sensing skin for quantitative imaging of damage in concrete. Smart Mater Struct 2014;23(8):085001. http://dx.doi.org/10.1088/0964-1726/23/8/085001. URL https://doi.org/10.1088%2F0964-1726%2F23%2F8%2F085001 .

[9] Downey A, Laflamme S, Ubertini F. Reconstruction of in-plane strain maps using hybrid dense sensor network composed of sensing skin. Meas Sci Technol 2016;27(12):124016. http://dx.doi.org/10.1088/0957-0233/27/12/124016. URL http://stacks.iop.org/0957-0233/27/i=12/a=124016 .

[10] Haber ZB, Saiidi MS, Sanders DH. Seismic performance of precast columns with mechanically spliced column-footing connections. ACI Struct J. 111 (3). http://dx.doi.org/10.14359/51686624. URL https://doi.org/10.14359%2F51686624.

[11] Loh K, Ryu D. Multifunctional materials and nanotechnology for assessing and monitoring civil infrastructures. In: Sensor technologies for civil infrastructures. Elsevier BV; 2014. p. 295–326. http://dx.doi.org/10.1533/9780857099136.295. URL https://doi.org/10.1533%2F9780857099136.295 .

[12] Ubertini F, Laflamme S, Ceylan H, Materazzi AL, Cerni G, Saleem H, et al. Novel nanocomposite technologies for dynamic monitoring of structures: a comparison between cement-based embeddable and soft elastomeric surface sensors. Smart Mater Struct 2014;23(4):045023. http://dx.doi.org/10.1088/0964-1726/23/4/045023. URL https://doi.org/10.1088%2F0964-1726%2F23%2F4%2F045023 .

[13] Han B, Ding S, Yu X. Intrinsic self-sensing concrete and structures: a review. Measurement 2015;59:110–28. http://dx.doi.org/10.1016/j.measurement.2014.09.048. URL https://doi.org/10.1016%2Fj.measurement.2014.09.048 .

[14] Han B, Sun S, Ding S, Zhang L, Yu X, Ou J. Review of nanocarbon-engineered multifunctional cementitious composites. Compos Part A: Appl Sci Manuf 2015;70:69–81. http://dx.doi.org/10.1016/j.compositesa.2014.12.002. URL https://doi.org/10.1016%2Fj.compositesa.2014.12.002 .

[15] Chen B, Liu J. Damage in carbon fiber-reinforced concrete, monitored by both electrical resistance measurement and acoustic emission analysis. Constr Build Mater 2008;22(11):2196–201. http://dx.doi.org/10.1016/j.conbuildmat.2007.08.004. URL https://doi.org/10.1016%2Fj.conbuildmat.2007.08.004 .

[16] Wen S, Chung D. Model of piezoresistivity in carbon fiber cement. Cem Concr Res 2006;36(10):1879–85. http://dx.doi.org/10.1016/j.cemconres.2006.03.029. URL https://doi.org/10.1016%2Fj.cemconres.2006.03.029 .

[17] Li H, Gang Xiao H, Ping Ou J. Effect of compressive strain on electrical resistivity of carbon black-filled cement-based composites. Cem Concr Compos 2006;28(9):824–8. http://dx.doi.org/10.1016/j.cemconcomp.2006.05.004. URL https://doi.org/10.1016%2Fj.cemconcomp.2006.05.004 .

[18] D'Alessandro A, Rallini M, Ubertini F, Materazzi AL, Kenny JM. Investigations on scalable fabrication procedures for self-sensing carbon nanotube cement-matrix composites for SHM applications. Cem Concr Compos 2016;65:200–13. http://dx.doi.org/10.1016/j.cemconcomp.2015.11.001. URL https://doi.org/10.1016%2Fj.cemconcomp.2015.11.001 .

[19] Azhari F, Banthia N. Cement-based sensors with carbon fibers and carbon nanotubes for piezoresistive sensing. Cem Concr Compos 2012;34(7):866–73. http://dx.doi.org/10.1016/j.cemconcomp.2012.04.007. URL https://doi.org/10.1016%2Fj.cemconcomp.2012.04.007 .

[20] Gdoutos EE, Konsta-Gdoutos MS, Danoglidis PA, Shah SP. Advanced cement based nanocomposites reinforced with MWCNTs and CNFs. Front Struct Civ Eng 2016;10(2):142–9. http://dx.doi.org/10.1007/s11709-016-0342-1. URL https://doi.org/10.1007%2Fs11709-016-0342-1 .

[21] García-Macías E, D'Alessandro A, Castro-Triguero R, Pérez-Mira D, Ubertini F. Micromechanics modeling of the electrical conductivity of carbon nanotube cement-matrix composites. Compos Part B: Eng 2017;108:451–69. http://dx.doi.org/10.1016/j.compositesb.2016.10.025. URL https://doi.org/10.1016/j.compositesb.2016.10.025 .

[22] Wang S, Chung D. Self-sensing of flexural strain and damage in carbon fiber polymer-matrix composite by electrical resistance measurement. Carbon 2006;44(13):2739–51. http://dx.doi.org/10.1016/j.carbon.2006.03.034. URL https://doi.org/10.1016%2Fj.carbon.2006.03.034 .

[23] Downey A, Garcia-Macias E, D'Alessandro A, Laflamme S, Castro-Triguero R, Ubertini F. Continuous and embedded solutions for SHM of concrete structures using changing electrical potential in self-sensing cement-based composites. In: Wu HF, Gyekenyesi AL, Shull PJ, Yu T-Y, editors. Nondestructive characterization and monitoring of advanced materials, aerospace, and civil infrastructure 2017. SPIE; 2017. http://dx.doi.org/10.1117/12.2261427. p. 101691G-1.

[24] Hou T-C, Lynch JP. Electrical impedance tomographic methods for sensing strain fields and crack damage in cementitious structures. J Intell Mater Syst Struct 2008;20(11):1363–79. http://dx.doi.org/10.1177/1045389x08096052. URL https://doi.org/10.1177%2F1045389x08096052 .

[25] Hou T-C, Loh KJ, Lynch JP. Spatial conductivity mapping of carbon nanotube composite thin films by electrical impedance tomography for sensing applications. Nanotechnology 2007;18(31):315501. http://dx.doi.org/10.1088/0957-4484/18/31/315501. URL https://doi.org/10.1088%2F0957-4484%2F18%2F31%2F315501 .

[26] Fu X, Ma E, Chung D, Anderson W. Self-monitoring in carbon fiber reinforced mortar by reactance measurement. Cem Concr Res 1997;27(6):845–52. http://dx.doi.org/10.1016/s0008-8846(97)83277-2. URL https://doi.org/10.1016%2Fs0008-8846%2897%2983277-2 .

[27] D'Alessandro A, Ubertini F, Materazzi AL, Laflamme S, Porfiri M. Electromechanical modelling of a new class of nanocomposite cement-based sensors for structural health monitoring. Struct Health Monit 2014;14 (2):137–47. http://dx.doi.org/10.1177/1475921714560071. URL https://doi.org/10.1177%2F1475921714560071 .

[28] Han B, Zhang K, Yu X, Kwon E, Ou J. Electrical characteristics and pressure-sensitive response measurements of carboxyl MWNT/cement composites. Cem Concr Compos 2012;34(6):794–800. http://dx.doi.org/10.1016/j.cemconcomp.2012.02.012. URL https://doi.org/10.1016%2Fj.cemconcomp.2012.02.012 .

[29] Han B, Yu X, Kwon E. A self-sensing carbon nanotube/cement composite for traffic monitoring. Nanotechnology 2009;20(44):445501. http://dx.doi.org/10.1088/0957-4484/20/44/445501. URL https://doi.org/10.1088%2F0957-4484%2F20%2F44%2F445501 .

[30] Chung DDL. Piezoresistive cement-based materials for strain sensing. J Intell Mater Syst Struct 2002;13(9):599–609. http://dx.doi.org/10.1106/104538902031861. URL https://doi.org/10.1106%2F104538902031861 .

[31] Wen S, Chung D. Cement-based materials for stress sensing by dielectric measurement. Cem Concr Res 2002;32(9):1429–33. http://dx.doi.org/10.1016/

s0008-8846(02)00789-5. URL https://doi.org/10.1016%2Fs0008-8846%2802%2900789-5 .
[32] Sun M, Liu Q, Li Z, Hu Y. A study of piezoelectric properties of carbon fiber reinforced concrete and plain cement paste during dynamic loading. Cem Concr Res 2000;30(10):1593–5. http://dx.doi.org/10.1016/s0008-8846(00)00338-0. URL https://doi.org/10.1016%2Fs0008-8846%2800%2900338-0 .
[33] Azhari F. Cement-based sensors for structural health monitoring [Ph.D. thesis]. University of British Columbia; 2008. http://dx.doi.org/10.14288/1.0063120. URL https://doi.org/10.14288/1.0063120.
[34] Loh KJ, Gonzalez J. Cementitious composites engineered with embedded carbon nanotube thin films for enhanced sensing performance. 11th international conference on damage assessment of structures, vol. 628. IOP Publishing; 2015. p. 012042. http://dx.doi.org/10.1088/1742-6596/628/1/012042. URL http://dx.doi.org/https://doi.org/10.1088%2F1742-6596%2F628%2F1%2F012042 .
[35] Downey A, D'Alessandro A, Ubertini F, Laflamme S, Geiger R. Biphasic DC measurement approach for enhanced measurement stability and multi-channel sampling of self-sensing multi-functional structural materials doped with carbon-based additives. Smart Mater Struct 2017;26(6):065008. http://dx.doi.org/10.1088/1361-665x/aa6b66. URL https://doi.org/10.1088/1361-665x/aa6b66 .
[36] Tersoff J. Contact resistance of carbon nanotubes. Appl Phys Lett 1999;74(15):2122–4. http://dx.doi.org/10.1063/1.123776. URL https://doi.org/10.1063%2F1.123776 .
[37] Materazzi AL, Ubertini F, D'Alessandro A. Carbon nanotube cement-based transducers for dynamic sensing of strain. Cem Concr Compos 2013;37:2–11. http://dx.doi.org/10.1016/j.cemconcomp.2012.12.013. URL https://doi.org/10.1016%2Fj.cemconcomp.2012.12.013 .
[38] Han B, Ou J. Embedded piezoresistive cement-based stress/strain sensor. Sens Actuat A: Phys 2007;138(2):294–8. http://dx.doi.org/10.1016/j.sna.2007.05.011. URL https://doi.org/10.1016/j.sna.2007.05.011 .
[39] García-Macías E, D'Alessandro A, Castro-Triguero R, P'erez-Mira D, Ubertini F. Micromechanics modeling of the uniaxial strain-sensing property of carbon nanotube cement-matrix composites for shm applications. Compos Struct 2017;163:195–215. http://dx.doi.org/10.1016/j.compstruct.2016.12.014. URL https://doi.org/10.1016/j.compstruct.2016.12.014 .
[40] Xiao H, Li H, Ou J. Modeling of piezoresistivity of carbon black filled cement-based composites under multi-axial strain. Sens Actuat A: Phys 2010;160(1–2):87–93. http://dx.doi.org/10.1016/j.sna.2010.04.027. URL https://doi.org/10.1016/j.sna.2010.04.027 .
[41] Han B, Guan X, Ou J. Electrode design, measuring method and data acquisition system of carbon fiber cement paste piezoresistive sensors. Sens Actuat A: Phys 2007;135(2):360–9. http://dx.doi.org/10.1016/j.sna.2006.08.003. URL https://doi.org/10.1016/j.sna.2006.08.003 .
[42] Paolo Nenzi HV. Ngspice users manual - Version 26. Paolo Nenzi, Holger Vogt, USA; 2014.
[43] Hibbit, Karlsson, Sorensen. ABAQUS/Standard Analysis User's Manual, Hibbit, Karlsson, Sorensen Inc., USA; 2007.